Hindawi
Journal of Electrical and Computer Engineering
Volume 2023, Article ID 7907782, 18 pages
https://doi.org/10.1155/2023/7907782

Research Article

Comparative Study of Two Nonlinear Control Strategies of Induction Motors considering Heating and Magnetic Saturation

Mustapha Es-Semyhy, Abdellfattah Ba-Razzouk, Mustapha El Haroussi, and Mhamed Madark

Mathematics, Computer and Engineering Sciences Laboratory, Systems Analysis, and Information Processing Team, Faculty of Science and Technology, Hassan 1st University, Settat, Morocco

Correspondence should be addressed to Mustapha Es-Semyhy; mustaphaessemyhy@gmail.com

Received 11 April 2023; Revised 10 June 2023; Accepted 8 August 2023; Published 21 August 2023

Academic Editor: Antonio J. Marques Cardoso

Feedback linearization technique (FLT) linearizes the model of induction machine (IM). This actuator suffers from the variation of its inductances due to saturation and resistances due to joule and skin effects. Sliding-mode control (SMC) is widely recognized as a robust technique against parametric variations of IM. This control strategy has the advantage of being simple to implement and requires only a simple flux observer. This explains the use of FLT and SMC in this work to control an IM while taking into account the magnetic saturation and heating of the IM. Simulation results, conducted in a MATLAB/Simulink environment, demonstrate the relevance and efficiency of the proposed control schemes.

1. Introduction

Induction machine (IM), as the name dictates, is a strongly inductive machine that allows the transformation of electrical energy into mechanical energy and vice versa. By nature, an IM is a strongly nonlinear system due to its inductive properties. Field-orientation techniques (FOC) allow simplifying the machine by making the flux and the torque dependent only on the direct and quadrature components of the stator currents [1]. However, FOC is sensitive to parameters variations [2]. Rotor resistance variation is the main problem that causes the loss of the decoupling between flux and torque [3]. Several solutions have been proposed in the literature to estimate the electrical parameters of IM. Rotor time constant (L_r/R_r) estimator has been proposed for an IM without saturation in [2], and identification of all IM parameters was presented in [4–7]. Magnetic saturation can also affect the inductances of IM, causing their variation. Several works have studied the effect of magnetic saturation in IM [8–11] to understand the behavior of the IM in the saturation area. These studies show that the best performances can be achieved when saturation is taken into account.

To extract maximum torque from IM, adaptive linear and nonlinear control laws have been proposed. To take into account the magnetic saturation of IM, the synthesis of nonlinear control laws is necessary. Several control laws are proposed and experimentally verified in the literature. For example, a PID controller is used in [2, 3, 6] with adaptation of some parameters. Advanced control laws were also applied to IM such as fuzzy logic [12, 13], backstepping technique [14–17], artificial neural networks (ANNs) [18–21], sliding mode (SM) [22–26], feedback linearization technique (FLT) [27, 28], and more. For sensorless control of IM without saturation phenomena, the authors in [12] suggest a model reference adaptive system (MRAS) speed estimator that uses type-1 and type-2 fuzzy logic controllers,

with the type-2 fuzzy logic controller being proposed to handle higher degrees of uncertainty and improve performance under various operating conditions. In [13], the authors suggest a fuzzy adaptive PI-sliding-mode controller for controlling the speed of IM. However, it assumes that the parameters are constant and ignores the effects of magnetic saturation. In [14], the speed control of IM using a backstepping design is proposed and compared to conventional PID control, but without considering the saturation effect. An adaptive backstepping-based nonlinear controller incorporating the iron loss is developed under the parameter uncertainties [15], and with a recursive online estimation of the rotor time constant and load torque [16], nonetheless, the variation of inductances is ignored. In [17], a maximum torque per ampere (MTPA) method based on the backstepping controller is presented for IM drives, taking into account the effects of both iron loss and saturation; however, the saturation of the main flux path was defined as a function of magnetizing current without physical meaning. In [18–21], the authors introduce the artificial neural networks (ANNs) for the control of IM using FOC principles, but they require data for training and consume a lot of memory resources. The authors in [22] present a model-based loss-minimization approach, which is combined with a backstepping direct torque control of the IM and describes a sliding-mode rotor flux observer to calculate the rotor speed, rotor time constant, and rotor flux space vector simultaneously. The authors in [23] use the proportional integral type SM switching surfaces to control the stator flux and torque of IM. The motor iron losses are modeled by a shunt rotor speed-dependent core resistance, but the saturation effect is not discussed. A sliding-mode controller is proposed to compensate for the uncertainties including parameter variations [24], but this strategy is applied to a linear induction motor (LIM) drive system without saturation effects. A suggested SMC-based model predictive control (MPC) scheme combines the advantages of SMC and MPC to develop a robust and flexible system that enhances tracking performance and torque ripple reductions [25] but the robustness concerning the variation of certain parameters is not discussed. Authors in [26] present the use of a higher-order sliding-mode scheme based on a super-twisting algorithm for sensorless control of IM, neglecting magnetic saturations.

When applying such nonlinear control laws, some assumptions are made which allow for obtaining interesting performances. Recently, in [27], the authors have developed a control law based on the feedback linearization technique (FLT) for saturated and unsaturated IM described in [10]. The shape of the magnetizing curve of IM has suggested its representation as the sum of an exponential function with a linear one [27]. This nonlinear function has three parameters to be determined. These parameters have a physical meaning [27, 29] which justifies the choice of this type of interpolation. However, the performance of the FLT controller depends strongly on the variation of the rotor and stator resistance (heating). In addition, estimation of the load torque is necessary to calculate the control voltages. The robustness problem motivates us to propose and synthesize a sliding-mode control (SMC) law in this paper. Contrary to FLT, the load torque in SMC is not necessary to estimate. The robustness of these two control laws against rotor resistance variation is discussed and compared.

This paper is organized as follows: Section 2 presents the mathematical model of the IM taking magnetic saturation into account. In Section 3, a new rotor flux model is developed that considers the machine's saturation, and a new inductance is defined. Section 4 describes the design of a feedback linearization technique (FLT) for controlling both the speed and rotor flux. In Section 5, a sliding-mode control (SMC) is proposed for the same purpose. Simulation results for both control strategies are presented in Section 6, with constant and variable rotor resistance. Section 7 provides the simulation configuration and nominal characteristics of the IM used in this study. Finally, Section 7 offers conclusions based on the findings.

For the symbols used in this paper, the reader can refer to Table 1.

2. Modeling of the Induction Machine considering the Magnetic Saturation

A dynamic model of IM taking into account the magnetic saturation of the iron core was introduced in [10] for direct torque control (DTC). The state space form of this model is described by [27] for the synthesis of a control law which combines the principles of rotor flux orientation and feedback linearization. This linearization is derived from [30] for induction motors (IM) and from [28] for linear induction motors (LIM). Nonlinear observers of the stator and magnetizing currents are studied and experimentally verified by [29] in the stationary reference frame. Based on the state model used in these papers, the robustness of the feedback linearization (FLT) control on the speed and torque performances, with respect to the variation of the rotor resistance, is compared to sliding-mode control (SMC).

Starting from the IM state model given by [27] in a reference frame (x, y) (general reference frame) rotating at speed ω_g, this model is given by

Table 1: List of symbols.

Symbols	Designation
u_{sx}, u_{sy}	Stator voltages in the rotor flux-oriented reference frame
i_{sx}, i_{sy}	Stator currents in the rotor flux-oriented reference frame
$i_{mr}, i_{mr}^{\text{ref}}$	Rotor magnetizing current, its reference (A) in the rotor flux-oriented reference frame
$\lvert\Psi_r\rvert = L_m\lvert i_{mr}\rvert$	Rotor flux magnitude (Wb)
L_m	Magnetizing inductance (H)
$L_s = L_{s\sigma} + L_m$	Stator inductance (H)
$L_r = L_{r\sigma} + L_m$	Rotor inductance (H)
$L_{s\sigma}, L_{r\sigma}$	Rotor leakage inductance (H)
$R_s\,(R_r)$	Stator (rotor) resistance (Ω)
T_r, T_r^*	Rotor time constant, modified rotor time constant
$\omega_r, \omega_r^{\text{ref}}$	Electrical speed of the rotor and its reference (rad/s)
ω_g	Rotating speed of a general reference frame (x, y)
T_{em}, T_L	Electromagnetic torque (Nm), load torque (Nm)
$\sigma = 1 - L_m^2/L_sL_r$	Total leakage factor
J_m	Inertia moment (kg·m^2)
p	Pole pairs
FLT	Feedback linearization technique
SMC	Sliding-mode control

$$\frac{\mathrm{d}i_{sx}}{\mathrm{d}t} = -c_1 i_{sx} + \left(\omega_g + c_2 T_r\left(\omega_g - \omega_r\right)\right) i_{sy} + c_3 i_{mrx} - \left(\left(c_3 T_r - a_{21}^* f_1 T_r^*\right)\omega_g - c_3 T_r \omega_r\right) i_{mry} - c_2 \frac{i_{\text{sx}}^2}{i_{mrx}} + f_1 u_{sx}, \tag{1}$$

$$\frac{\mathrm{d}i_{sy}}{\mathrm{d}t} = -c_1 i_{sy} - \left(\omega_g + c_2 T_r\left(\omega_g - \omega_r\right)\right) i_{sx} + c_3 i_{mry} + \left(\left(c_3 T_r - a_{21}^* f_1 T_r^*\right)\omega_g - c_3 T_r \omega_r\right) i_{mrx} - c_2 \frac{i_{\text{sy}}^2}{i_{mrx}} + f_1 u_{sy}, \tag{2}$$

$$\frac{\mathrm{d}i_{mrx}}{\mathrm{d}t} = a_{22}^* i_{sx} - a_{22}^* i_{mrx} + a_{22}^* T_r\left(\omega_g - \omega_r\right) i_{mry}, \tag{3}$$

$$\frac{\mathrm{d}i_{mry}}{\mathrm{d}t} = a_{22}^* i_{sy} - a_{22}^* i_{mry} - a_{22}^* T_r\left(\omega_g - \omega_r\right) i_{mrx}, \tag{4}$$

$$\frac{\mathrm{d}\omega_r}{\mathrm{d}t} = -a_{33}\omega_r + f_3\left(i_{mrx} i_{sy} - i_{mry} i_{sx}\right) - f_4 T_L. \tag{5}$$

The magnetizing current vector magnitude $|i_{mr}| = \sqrt{i_{mrx}^2 + i_{mry}^2}$ will be oriented along the x-axis of the rotating reference frame. The rotating speed ω_g is equal to the case of unsaturated machine [27].

$$\omega_g = \omega_r + a_{22}\frac{i_{sy}}{i_{mrx}}. \tag{6}$$

The magnitude of the magnetizing current vector will be equal to $|i_{mr}| = i_{mrx}$. It is useful to note that the speed of rotation ω_g is equal to the case of the unsaturated machine. This means that the saturation effects only change the magnitude or vector of the flux rotor, while its angle remains unchanged [27].

By substituting (6) in (1)–(4) and setting $i_{mry}(0) = 0$, the state model (1)–(5) of IM, taking into account the magnetic saturation, in the rotor flux-oriented reference frame (x, y) can be written as follows:

$$\frac{\mathrm{d}i_{sx}}{\mathrm{d}t} = -c_1 i_{sx} + \omega_r i_{sy} + (a_{22} + c_2)\frac{i_{sy}^2}{i_{mrx}} - c_2\frac{i_{sx}^2}{i_{mrx}} + c_3 i_{mrx} + f_1 u_{sx}, \tag{7}$$

$$\frac{\mathrm{d}i_{sy}}{\mathrm{d}t} = -(a_{11} - c_2)i_{sy} - \omega_r i_{sx} - (a_{22} + c_2)\frac{i_{sx}i_{sy}}{i_{mrx}} - \frac{f_1 a_{21}}{a_{22}}\omega_r i_{mrx} - c_2\frac{i_{sy}^2}{i_{mrx}} + f_1 u_{sy}, \tag{8}$$

$$\frac{di_{mrx}}{dt} = a_{22}^* i_{sx} - a_{22}^* i_{mrx}, \tag{9}$$

$$\frac{d\omega_r}{dt} = -a_{33}\omega_r + f_3 i_{mrx} i_{sy} - f_4 T_L. \tag{10}$$

We add to this model the equation of the electromagnetic torque, expressed in the rotating reference frame (x, y):

$$T_{em} = f_2 . i_{mrx} . i_{sy}. \tag{11}$$

The coefficients appearing in the IM model are defined by

$$a_{11}^* = \frac{R_s}{\sigma L_s} + \frac{1-\sigma}{\sigma T_r^*}, \tag{12.a}$$

$$a_{12}^* = \frac{1}{\sigma L_s T_r^*}, \tag{12.b}$$

$$a_{21}^* = L_s\frac{1-\sigma}{T_r^*}, \tag{12.c}$$

$$a_{22} = \frac{1}{T_r}, \tag{12.d}$$

$$a_{22}^* = \frac{1}{T_r^*}, \tag{12.e}$$

$$a_{33} = \frac{b_r}{J_m}, \tag{12.f}$$

$$f_1 = \frac{1}{\sigma L_s}, \tag{12.g}$$

$$f_2 = \frac{3}{2}p\frac{L_m^2}{L_r}, \tag{12.h}$$

$$f_3 = \frac{p}{J_m}f_2, \tag{12.i}$$

$$\Delta L = L - L_m, \tag{12.j}$$

$$\Delta L^* = \frac{L_{\sigma r}^2}{L_r^2}\Delta L, \tag{12.k}$$

$$c_1 = a_{11}^* + a_{12}^*(\Delta L - 2\Delta L^*), \tag{12.l}$$

$$c_2 = a_{12}^*\Delta L^*, \tag{12.m}$$

$$c_3 = a_{21}^* f_1 + a_{12}^*(\Delta L - \Delta L^*). \tag{12.n}$$

For simplification, these parameters are grouped in a vector ″ par ″ defined by

$$par = [c_1\, c_2\, c_3\, a_{11}^* a_{12}^*\, a_{21}^*\, a_{22}^*\, f_1\, f_2\, f_3]^T. \tag{12.o}$$

Note: The parameters with "*" vary as a function of the magnetizing current magnitude $|i_{mr}|$ and indirectly as a function of time.

3. Rotor Flux Model Taking into Account the Saturation of the Machine

Several works have addressed the IM saturation effect in the literature. In [31], nonlinear functions are proposed to model the magnetizing inductance and the leakage inductance of the rotor. From experimental data, the authors in [17] used an interpolation function consisting of three (3) parameters to model the magnetic flux. This function is the basis for calculating two inductances: dynamic and static inductances, which will be incorporated into the parameters of IM. In [32], magnetizing inductance and stator and rotor leakage inductances are introduced, but it requires twelve (12) parameters to be determined which makes these inductances very difficult to exploit.

The work published in [27, 29, 33] has allowed experimentally verifying the rotor flux profile as a function of the rotor magnetizing current (see Figure 1).

As can be seen in Figure 1, the rotor flux can be described as a sum of an exponential function and a linear function [27, 29] as follows:

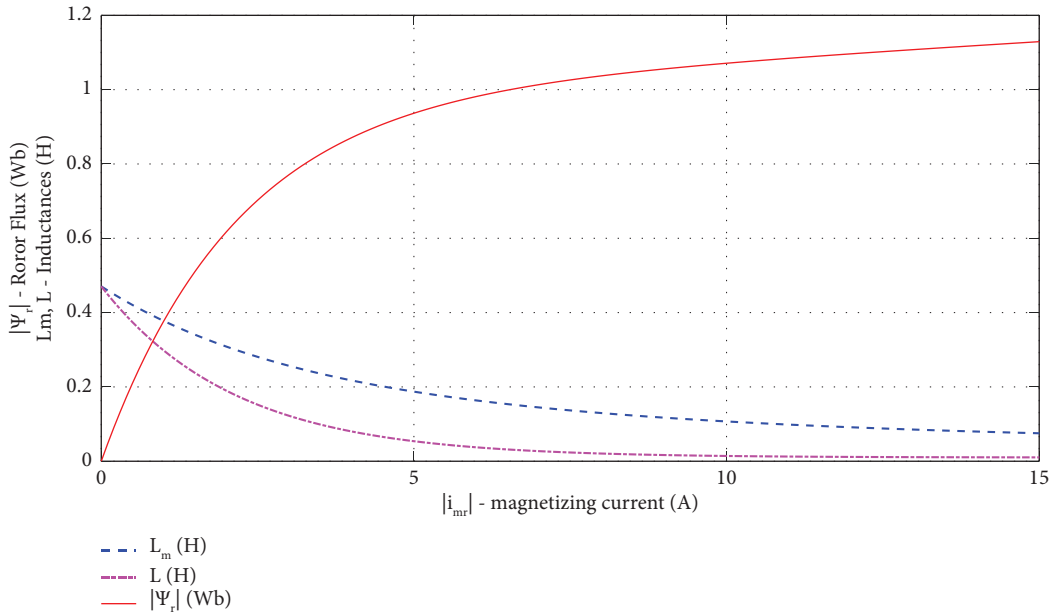

Figure 1: Typical magnetization curve of IM.

$$|\Psi_r| = \alpha\left(1 - e^{-\beta|i_{mr}|}\right) + \gamma|i_{mr}|. \tag{13}$$

The coefficients α, β, and γ were obtained by means of an optimal optimization (see [33]).

The magnetizing inductance L_m is defined by [10]

$$L_m = \frac{|\Psi_r|}{|i_{mr}|}. \tag{14}$$

A new inductance has been introduced in [10], called modified inductance, and is defined by

$$L = \frac{d|\Psi_r|}{d|i_{mr}|}. \tag{15}$$

From (11), the expressions of L_m and L are obtained analytically as follows:

$$L_m = \frac{\alpha\left(1 - e^{-\beta|i_{mr}|}\right)}{|i_{mr}|} + \gamma, \tag{16}$$

$$L = \alpha\beta e^{-\beta|i_{mr}|} + \gamma. \tag{17}$$

4. Feedback Linearization Technique (FLT)

From equations (7) and (8), the two linearizing and stabilizing control inputs u_{sx} and u_{sy} of the system are given by

$$u_{sx} = \frac{1}{f_1}\left(-\omega_r i_{sy} - (a_{22} + c_2)\frac{i_{sy}^2}{i_{mrx}} + c_2\frac{i_{sx}^2}{i_{mrx}} - c_3 i_{mrx} + v_x\right), \tag{18}$$

$$u_{sy} = \frac{1}{f_1}\left(-c_2 i_{sy} + \omega_r i_{sx} + (a_{22} + c_2)\frac{i_{sx} i_{sy}}{i_{mrx}} + \frac{f_1 a_{21}}{a_{22}}\omega_r i_{mrx} + c_2\frac{i_{sy}^2}{i_{mrx}} + v_y\right), \tag{19}$$

where v_x and v_y are additional control inputs that will be designed later.

As can be seen in model (7)–(10), the dynamics of torque and flux is not decoupled in each working condition. Indeed, the decoupling between torque and flux only works if the machine is operating at constant flux; otherwise, the speed dynamics has a nonlinearity with respect to the inputs, and another important coupling between torque and magnetizing current comes from the dependence of the model coefficients on the current i_{mr} due to saturation effects. For this reason, two variables will be introduced in the IM model. The input-output feedback law of the model will be applied to the new model [27].

Let us define a new state variable "a" called angular acceleration, instead of i_{sy} as follows:

$$a = -a_{33}\omega_r + f_3 i_{mrx} i_{sy} - f_4 T_L. \tag{20}$$

Assuming that the change in load torque is sufficiently slow, i.e., $\dot{T}_L = 0$ [27, 34], then the derivative of a can be written as follows:

$$\begin{aligned}\frac{\mathrm{d}a}{\mathrm{d}t} &= -a_{33}a + \frac{\mathrm{d}f_3}{\mathrm{d}t} i_{mrx} i_{sy} + f_3 \frac{\mathrm{d}i_{mrx}}{\mathrm{d}t} i_{sy} + f_3 \frac{\mathrm{d}i_{sy}}{\mathrm{d}t} i_{mrx} \\ &= -a_{33}a + \frac{df_3}{di_{mrx}} a_{22}^* (i_{sx} - i_{mrx}) i_{mrx} i_{sy} + f_3 a_{22}^* (i_{sx} - i_{mrx}) i_{sy} - f_3 a_{11} i_{sy} + f_3 i_{mrx} v_{y.}\end{aligned} \tag{21}$$

By analyzing (21), it is easy to see that the feedback term that linearizes the speed dynamics can be defined as follows:

$$v_y = \frac{a_{33}a}{f_3 i_{mrx}} - \frac{df_3}{di_{mrx}} \frac{a_{22}^* (i_{sx} - i_{mrx}) i_{sy}}{f_3} - a_{22}^* \frac{i_{sx} i_{sy}}{i_{mrx}} + (a_{22}^* + a_{11}) i_{sy} + \frac{1}{f_3 i_{mrx}} v_y'. \tag{22}$$

Finally, we define a new state variable $v_{i_{mrx}}$ as follows:

$$v_{i_{mrx}} = a_{22}^* (i_{sx} - i_{mrx}). \tag{23}$$

Then, we derive $v_{i_{mrx}}$ with respect to time, which gives

$$\begin{aligned}\frac{dv_{i_{mrx}}}{dt} &= \frac{da_{22}^*}{dt} (i_{sx} - i_{mrx}) + a_{22}^* \left(\frac{di_{sx}}{dt} - \frac{di_{mrx}}{dt} \right) \\ &= \frac{da_{22}^*}{di_{mrx}} (a_{22}^* (i_{sx} - i_{mrx})) (i_{sx} - i_{mrx}) + a_{22}^* (-c_1 i_{sx} + v_x) - a_{22}^* \frac{di_{mrx}}{dt} \\ &= a_{22}^* \left(\frac{da_{22}^*}{di_{mrx}} (i_{sx} - i_{mrx})^2 - (c_1 + a_{22}^*) i_{sx} + a_{22}^* i_{mrx} + v_x \right).\end{aligned} \tag{24}$$

Looking at (24), the feedback term that linearizes the dynamics of the magnetizing current can be defined as follows:

$$v_x = \frac{1}{a_{22}^*} \left(-\frac{da_{22}^*}{di_{mrx}} (i_{sx} - i_{mrx})^2 + (c_1 + a_{22}^*) i_{sx} - a_{22}^* i_{mrx} + v_x' \right). \tag{25}$$

Replacing (22) in (21) and (25) in (24), model (7)–(10) can finally be written as follows:

$$\frac{di_{mrx}}{dt} = v_{i_{mrx}}, \tag{26}$$

$$\frac{dv_{i_{mrx}}}{dt} = v_x', \tag{27}$$

$$\frac{d\omega_r}{dt} = a, \tag{28}$$

$$\frac{da}{dt} = v_y'. \tag{29}$$

Model (26)–(29) are the linearized model of the induction motor, with a decoupled dynamic between the speed and the magnetizing current, taking into account the magnetic saturation [27].

In order that i_{mrx} and ω_r follow their respective references i_{mr}^{ref} and ω_r^{ref}, we introduce the following two errors:

$$e_1 = \omega_r - \omega_r^{\mathrm{ref}}, \tag{30}$$

$$e_2 = i_{mrx} - i_{mr}^{\mathrm{ref}}. \tag{31}$$

The input signals v_x' and v_y' are then designed as follows:

$$v_x' = -k_{1m}.e_2 - k_{2m}.\dot{e}_2 + \ddot{i}_{mr}^{\mathrm{ref}}, \tag{32}$$

$$v_y' = -k_{1\omega}.e_1 - k_{2\omega}.\dot{e}_1 + \ddot{\omega}_r^{\mathrm{ref}}. \tag{33}$$

Coefficients $k_{1m}, k_{2m}, k_{1\omega}$et $k_{2\omega}$ are parameters of the control. An appropriate choice of these parameters allows a good tracking of desired trajectories for speed and rotor flux.

Now, if we consider the closed-loop stability of this strategy and replace (27) and (29) by the expressions of the

control commands v_x' and v_y', we obtain the following homogeneous differential equations:

$$\ddot{e_1} + k_{2\omega}\dot{e_1} + k_{1\omega}e_1 = 0, \tag{34}$$

$$\ddot{e_2} + k_{2m}\dot{e_2} + k_{1m}e_2 = 0. \tag{35}$$

If equations (34) and (35) are Hurwitz polynomials, the system is stable.

The canonical form of a second-order system is as follows:

$$s^2 + 2\xi\omega_n s + \omega_n^2 = 0, \tag{36}$$

where s is the Laplace variable, ξ is the damping factor, and ω_n is the natural pulsation.

Knowing the profile of the desired references, we can determine the parameters of the state feedback using the following expressions:

$$\begin{cases} k_{1m} = \omega_{mn}^2 \\ k_{2m} = 2\xi_{mn}\omega_{mn} \end{cases} \tag{37}$$

$$\begin{cases} k_{1\omega} = \omega_{\omega n}^2 \\ k_{2\omega} = 2\xi_{\omega n}\omega_{\omega n}. \end{cases} \tag{38}$$

Notes:

(i) We note the dependence of the machine parameters on the magnetizing current i_{mrx} and therefore these parameters are time varying.

(ii) The magnetizing current observer is designed from equation (10) by replacing i_{mrx} by its estimate $\hat{i}_{mrx}$

Figure 2 shows the complete block diagram of IM and feedback linearization (FLT) controller.

5. Sliding Mode Based on Exact Linearization (SMC)

In practice, all the parameters of IM vary, due to saturation (variation of inductances) and heating (variation of rotor and stator resistances).

Variations in rotor and stator resistances will be considered as disturbances in each state variable. Models (7)–(10) become

$$\frac{di_{sx}}{dt} = f_{sx}(x) + f_1.u_{sx} + d_{sx}, \tag{39}$$

$$\frac{di_{sy}}{dt} = f_{sy}(x) + f_1.u_{sy} + d_{sy}, \tag{40}$$

$$\frac{di_{mrx}}{dt} = a_{22}^*\left(i_{sx} - i_{mrx}\right) + d_{mr,} \tag{41}$$

$$\frac{d\omega_r}{dt} = f_3 i_{mrx} i_{sy} + d_L, \tag{42}$$

where $x = [i_{sx}\, i_{sy}\, i_{mrx}\, \omega_r]^T$ is the state vector. We derive

$$f_{sx}(x) = -c_1 i_{sx} + \omega_r i_{sy} + (a_{22} + c_2)\frac{i_{sy}^2}{i_{mrx}} - c_2\frac{i_{sy}^2}{i_{mrx}} + c_3 i_{mrx}, \tag{43}$$

$$f_{sy}(x) = -(a_{11} - c_2)i_{sy} - \omega_r i_{sx} - (a_{22} + c_2)\frac{i_{sx}i_{sy}}{i_{mrx}} - \frac{f_1 a_{21}}{a_{22}}\omega_r i_{mrx} + c_3 i_{mry} - c_2\frac{i_{sy}^2}{i_{mrx}}, \tag{44}$$

$$d_L = -a_{33}\omega_r - f_4 T_L. \tag{45}$$

Terms d_{sx}, d_{sy}, and d_{mr} are added to compensate uncertainties caused by rotor and stator resistances variation. The term d_L is used to model the disturbances coming from the load and friction torque: $d_{sx} = d_{sx}(R_r, R_s)$, $d_{sy} = d_{sy}(R_r, R_s)$, $d_{mr} = d_{mr}(R_r)$, and $d_L = d_L(T_l, a_{33}) = c^{ste}$.

Synthesis of the sliding-mode control law is based on input-output linearization. To obtain the relation between ω_r and u_{sy}, we differentiate ω_r until the command appears:

$$\begin{aligned} \frac{d^2\omega_r}{dt^2} &= \left(\frac{df_3}{di_{mrx}}i_{mrx}i_{sy} + f_3 i_{sy}\right)\frac{di_{mrx}}{dt} + f_3 f_{sy}(x)i_{mrx} + f_1 f_3 i_{mrx}\, u_{sy} + f_3 i_{mrx}\, d_{sy} + \dot{d}_L \\ &= F_{\omega r}(x) + f_1 f_3 i_{mrx}\, u_{sy} + d_{\omega r}(x), \end{aligned} \tag{46}$$

where

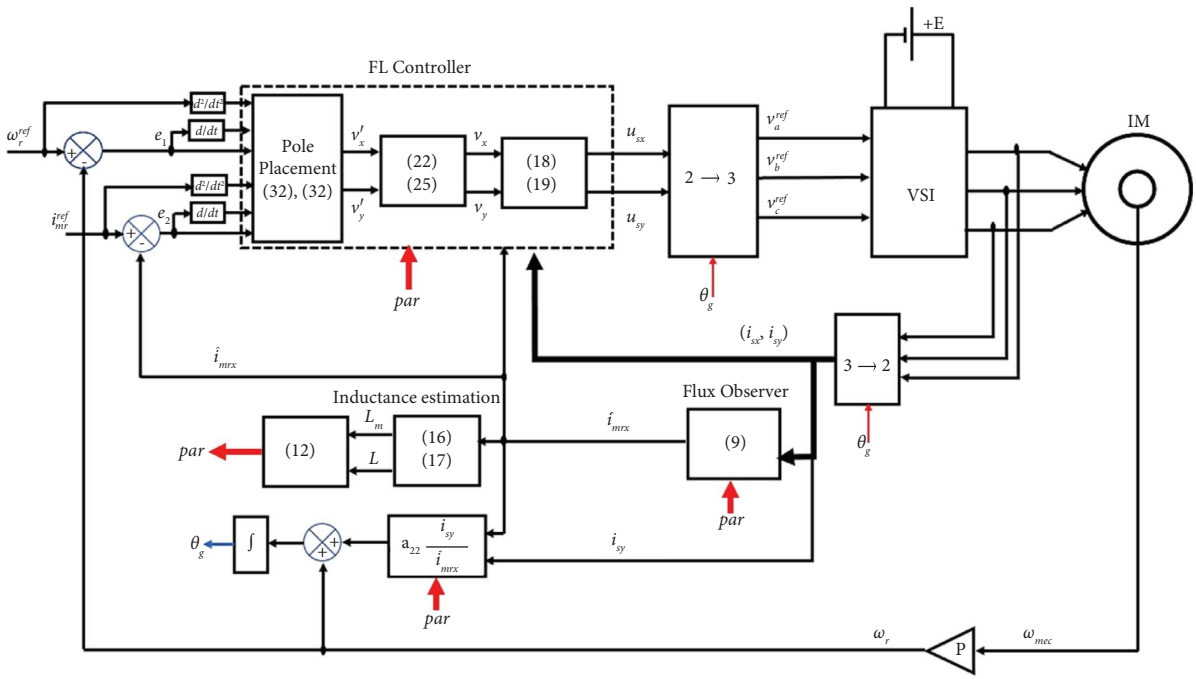

Figure 2: Block diagram of the feedback linearization technique (FLT) control.

$$F_{\omega r}(x) = \left(\frac{df_3}{di_{mrx}}.i_{mrx}.i_{sy} + f_3 i_{sy}\right).\frac{di_{mrx}}{dt} + f_3.f_{sx}(x).i_{mrx}, \tag{47}$$

$$d_{\omega r}(x) = f_3 i_{mrx} d_{sy} + \dot{d}_L. \tag{48}$$

From (46), we deduce the control command u_{sy} as follows:

$$u_{sy} = \frac{1}{f_1 f_3 i_{mrx}}\left(-F_{\omega r}(x) + \mathrm{v}_{sy} - k_1 sgn(S_1)\right). \tag{49}$$

We define the speed error: $e_1 = \omega_r - \omega_r^{ref}$, and the sliding surface is selected as follows:

$$S_1 = \dot{e}_1 + \lambda_1 e_1. \tag{50}$$

With $\lambda_1 > 0$, v_{sy} is the intermediate command that will be chosen and defined later.

We define the Lyapunov function as follows:

$$V_1 = \frac{1}{2}S_1^2. \tag{51}$$

The derivative with respect to time is given by

$$\begin{aligned}\dot{V}_1 = S_1\dot{S}_1 &= S_1\left(F_{\omega r}(x) + f_1 f_3 i_{mrx}.u_{sy} + d_{\omega r}(x) - \ddot{\omega}_r^{ref} + \lambda_1\dot{e}_1\right)\\ &= S_1\left(\mathrm{v}_{sy} - k_1 sgn(S_1) + d_{\omega r}(x) - \ddot{\omega}_r^{ref} + \lambda_1\dot{e}_1\right).\end{aligned} \tag{52}$$

We choose

$$\mathrm{v}_{sy} = \ddot{\omega}_r^{ref} - \lambda_1\dot{e}_1. \tag{53}$$

Equation (52) becomes

$$\dot{\mathrm{V}}_1 = S_1\left(-k_1 sgn(S_1) + d_{\omega r}(x)\right) = -k_1|S_1| + d_{\omega r}(x)S_1 \le \left(-k_1 + D_{\omega r}\right)|S_1|. \tag{54}$$

The condition for that $\dot{\mathrm{V}}_1 \le -\eta_1|S_1|$ is to choose

$$k_1 = \eta_1 + D_{\omega r}. \tag{55}$$

To find η_1, we use the following reaching law:

$$\eta_1 = \frac{|S_1(0)|}{\tau_1}, \tag{56}$$

where $\tau_1 = 2\pi/\omega_{c1}$ is the reaching time and ω_{c1} is chosen to be equal to bandwidth, and then $D_{\omega r} \geq |f_3 i_{mrx} d_{sy} + \dot{d}_L| = f_3 |i_{mrx} d_{sy}|$ because $\dot{d}_L = 0$ and f_3 is always positive.

The same procedure will be applied for the synthesis of the current control law for i_{mrx}.

To obtain the relationship between i_{mrx} and u_{sx} we differentiate i_{mrx} until the command u_{sx}:

$$\begin{aligned}\frac{d^2 i_{mrx}}{dt^2} &= \left(\frac{da_{22}^*}{di_{mrx}}(i_{sx} - i_{mrx}) - a_{22}^*\right)\frac{di_{mrx}}{dt} + a_{22}^* f_{sx}(x) + a_{22}^* f_1 u_{sx} + a_{22}^* d_{sx} + \dot{d}_{mr} \\ &= F_r(x) + a_{22}^* f_1 u_{sx} + d_r(x),\end{aligned} \tag{57}$$

with

$$F_r(x) = \left(\frac{da_{22}^*}{di_{mrx}}(i_{sx} - i_{mrx}) - a_{22}^*\right)\frac{di_{mrx}}{dt} + a_{22}^* f_{sx}(x), \tag{58}$$

$$d_r(x) = a_{22}^* d_{sx} + \dot{d}_{mr}. \tag{59}$$

From (57), we deduce the following control command u_{sy}:

$$u_{sy} = \frac{1}{a_{22}^* f_1}\left(-F_r(x) + \mathrm{v}_{sx} - k_2 sgn(S_2)\right). \tag{60}$$

Defining the error $e_2 = i_{mrx} - i_{mr}^{ref}$ and selecting the new sliding surface as follows:

$$S_2 = \dot{e}_2 + \lambda_2 e_2, \tag{61}$$

with $\lambda_2 > 0$ v_{sx} is the intermediate command that will be chosen later.

Let us define the Lyapunov function as follows:

$$V_2 = \frac{1}{2} S_2^2. \tag{62}$$

The derivative with respect to time gives

$$\begin{aligned}\dot{\mathrm{V}}_2 = S_2\dot{S}_2 &= S_2\left(F_r(x) + \left(-F_r(x) + \mathrm{v}_{sx} - k_2 sgn(S_2)\right) + d_r(x) - \ddot{i}_{mr}^{\mathrm{ref}} + \lambda_2 \dot{e}_2\right) \\ &= S_1\left(\mathrm{v}_{sx} - k_2 sgn(S_2) + d_r(x) - \ddot{\omega}_r^{\mathrm{ref}} + \lambda_2 \dot{e}_2\right).\end{aligned} \tag{63}$$

We choose

$$\mathrm{v}_{sx} = \ddot{i}_{mr}^{\mathrm{ref}} - \lambda_2 \dot{e}_2. \tag{64}$$

Equation (63) becomes

$$\dot{V}_2 = S_2\left(-k_2 sgn(S_2) + d_r(x)\right) = -k_2|S_2| + d_r(x)S_2 \leq \left(-k_2 + D_r\right)|S_2| \leq 0. \tag{65}$$

To find η_2, we use the reaching law:

$$\eta_2 = \frac{|S_2(0)|}{\tau_2}. \tag{66}$$

The condition for that $\dot{V}_2 \leq -\eta_2|S_2|$ is to choose

$$k_2 = \eta_2 + D_r, \tag{67}$$

where $\tau_2 = 2\pi/\omega_{c2.}$ is the reaching time, $\omega_{c2} = 5.\omega_{c1}$, and $D_r \geq |f_3 i_{mrx} d_{sy} + \dot{d}_L| = f_3 |i_{mrx} d_{sy}|$.

Notes:

(i) Terms $D_{\omega r}$ and D_r are chosen large enough; in this work, we use the simulation tool to estimate their values.

(ii) To reduce the chattering problem, we replace the function $sgn(.)$ by $\tan h(.)$.

The block diagram of the sliding-mode control (SMC) is given in Figure 3.

6. Simulation Result

The simulations for this study were conducted using the MATLAB/Simulink environment, employing a sample time of $T_{sc} = 50\,\mu s$. This choice of sample time was made to account for the development of microcontrollers, such as DSP and FPGA, and to improve the accuracy of simulation results. It should be noted, however, that the physical system being studied is not simulated, and the digital computer only executes the control algorithm, requiring fewer calculations and allowing for lower sampling steps. The simulations employed the SPWM (sinusoidal PWM) technique based on the concept of "effective time" [35] and utilized the ode8 (Dormand-Prince) solver with a fixed step $T_s = 5\,\mu s$. The switching frequency was set at 2 kHz. Table 2 gives the nominal characteristics of the IM used in this paper.

6.1. Constant Rotor Resistance. First, the reference speed is set to $\omega_r^{\text{ref}} = 100\,rad/s$ and the magnetizing current to its nominal value ($i_{mr}^{\text{ref}} = 3.5\,A$). Based on linear systems theory, the coefficients of the FLT controller are chosen according to the following specifications: $\xi_{mn} = \xi_{\omega n} = 1$, $\omega_{\omega n} = 140$ rad/s, and $\omega_{mn} = 5.\omega_{\omega n} = 700$ rad/s shown in Table 3. For the SMC controller, the coefficients of the SMC controller are chosen according to the following specifications: $\tau_1 = 2\pi/\omega_{c1}$, $\lambda_1 = 140$ ras/s, $\tau_2 = 2\pi/\omega_{c2}$, $\lambda_2 = 5.\lambda_1$, $D_{\omega r} = 8.10^6$, and $D_r = 6.10^5$. Table 3 gives the coefficients of FLT and SMC used in simulations.

At time $t = 0.5$ s, nominal load torque $T_L = 14$ Nm is applied. Figure 4 shows the simulation result obtained by the FLT controller.

We notice that the FLT controller allows us to follow the rotor speed and its reference (Figure 4(a)). When the load torque T_L is applied (Figure 4(b)), there is a slight decrease in the speed controlled by FLT (Figure 4(d)). We can improve the accuracy of the FLT controller by increasing adjustment parameters $k_{1\omega}$ and $k_{2\omega}$. Note that FLT controller uses linear control techniques which allows to control the desired dynamics by specifying the parameters $\xi_{\omega n}$ and $\omega_{\omega n}$.

Electromagnetic torque developed by IM (Figure 4(b)) compensates the load torque applied at $t_1 = 0.5$ s. According to (11), the torque is a function of the magnetizing current i_{mrx} and the current i_{sy}. So, if the magnetizing current i_{mrx} is maintained constant and if the torque response is dynamically faster (by using a larger natural pulsation ω_{cm}), the control of the electromagnetic torque will be done only by the quadrature component i_{sy} (see Figure 5).

Figure 4(c) shows the magnetizing current (i_{mr}) and its reference in the FLT control case. When the IM parameters are constant, especially the rotor resistance (R_r), the magnetizing current error obtained by the FLT controller is about $10^{-3}\,A$ (Figure 4(e)). During transient operation, a decrease in magnetizing current is observed since the magnetizing inductance has also decreased in the same manner (Figure 4(f)).

Figure 5 gives the stator current i_{sx} and i_{sy}, in rotating reference frame (x, y) and the three-phase currents absorbed by the motor (i_{sa}, i_{sb}, andi_{sc}).

At steady state, $i_{sx} = i_{mrx} = 3.5\,A$ in the FLT controller case. This means that current i_{sx} allows controlling the magnetizing current i_{mr} while the quadrature current i_{sy} allows controlling the electromagnetic torque (it is the principle of field-oriented control (FOC)). The profile of currents i_{sx} and i_{sy} demonstrate these results (Figure 5). The corresponding stator's current waveform is shown in Figures 5(b) and 5(c).

The SMC controller can address the challenges of parameter variations in the field-oriented control (FOC) system. In addition, one advantage of SMC is its relative simplicity of implementation. Figure 6 shows the simulation results when the rotor resistance is assumed to be constant and equal to its nominal value.

Figure 6(a) shows that the SMC controllers give quasi-equivalent results as in the FLT case, except in the transient state. In steady state, Figure 6(d) clearly shows that SMC is more accurate than FLT controllers in terms of rotor speed.

The electromagnetic torque (Figure 6(b)) and magnetizing current (Figure 6(c)) are the same as those developed by the FLT controller (Figure 6(b)). However, the magnetizing current error (Figure 6(e)) obtained by SMC is lower than that obtained by FLT (see Figure 4(e)).

The direct i_{sx} and quadrature i_{sy} currents have the same values and profiles as those of FLT (Figure 6(g)), and the waveform of the three-phase stator currents shows the good quality of stator currents.

6.2. Variable Rotor Resistance. In practice, the stator and rotor resistance of IM varies according to the temperature (heat). Physically, the resistance varies at slow dynamics (large time constant compared to the rotor time constant). Now, assume that the rotor resistance varies according to the profile given in Figure 7. The choice of this profile (Figure 7) is just to test the dynamics and the robustness of the FLT controller. Regarding inductances, it is useful to note that all the inductances (L_m, L, L_s, L_r) of the machine are variable.

The reference speed and current are kept at $\omega_r^{\text{ref}} = 100$ rad/s and $i_{mr}^{\text{ref}} = 3.5\,A$, respectively. Similarly, at the time $t = 0.5$ s, the nominal load torque of 14 Nm is applied. Figure 8 shows the simulation results when the rotor resistance varies according to the profile in Figure 7.

In the first step, the rotor resistance value has been increased to $R_r = R_{rn}$, before the application of the load torque. At no load, the FLT controller allows following accurately the rotor speed. At $t_1 = 0.4$ s, when the rotor resistance increases to $2R_{rn}$, the rotor speed obtained by FLT remains equal to 100 rad/s. At $t_2 = 0.5$ s, the load torque is applied, and rotor resistor is maintained equal to $2R_{rn}$, and the speed controlled by FLT decreases to 94 rad/s. At $t_3 = 1$s, the rotor resistance is decreased to $0.2\,R_{rn}$, the speed increases to 104.5 rad/s. Furthermore, from $t_4 = 1.5$ s onwards, as the resistance is exponentially increased to $2.R_{rn}$, it is

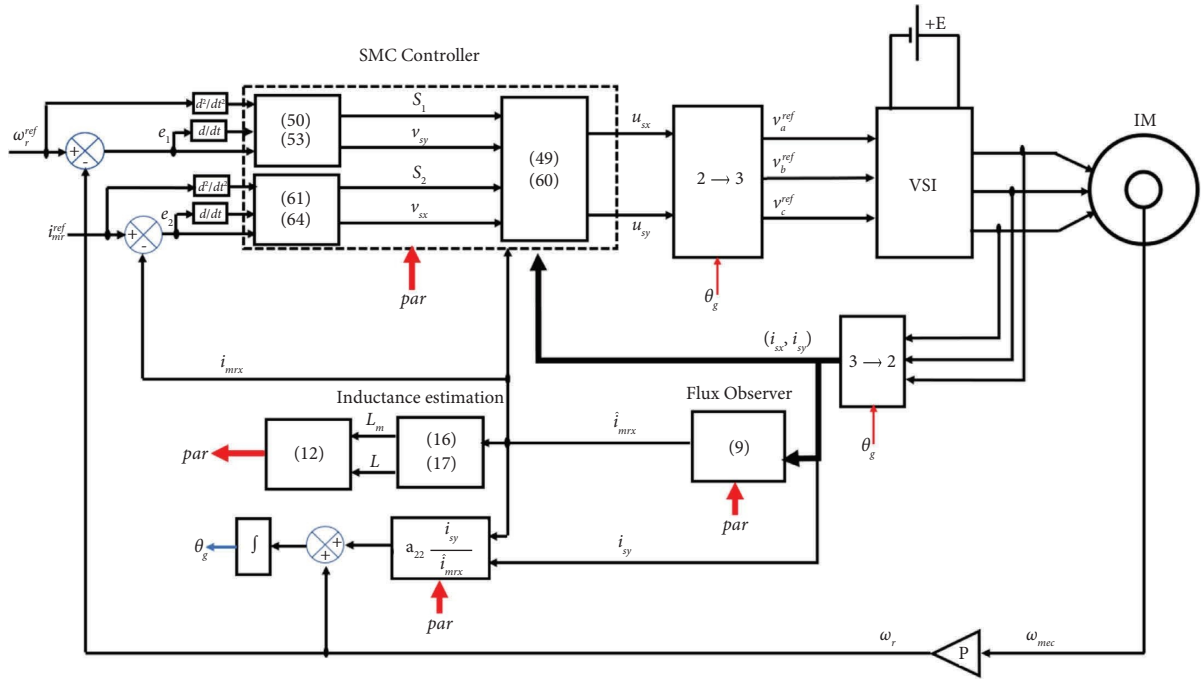

Figure 3: Block diagram of the sliding-mode control (SMC).

Table 2: Nominal values of IM.

Parameters	Values
Rated power P_{nom}	2.2 kW
Rated voltage V_{nom}	220 V
Rated frequency f_{nom}	50 Hz
Rated speed Ω_{nom}	1425 rpm
Rated torque $T_{\text{em,nom}}$	14 Nm
Pole pairs p	2
Power factor PF	0.75
Inertia moment J_m	0.0067 kg·m^2
E (DC BUS)	650 V
$L_{\sigma r} = L_{\sigma s}$	0.012 H
R_{sn}	2.90 Ω
R_{rn}	1.52 Ω

Table 3: The tuning parameters for both FTL and SMC controllers.

	FLT				SMC			
	Speed		Flux		Speed		Flux	
Parameter	$k_{1\omega}$	$k_{2\omega}$	k_{1m}	k_{2m}	k_1	λ_1	k_2	λ_2
	$4,78.10^4$	437.50	$1,20.10^6$	$2.19.10^3$	$8,31.10^6$	140	$8,65.10^5$	700

observed that the speed decreases exponentially in the case of FLT. This implies that a rapid increase in rotor resistance leads to a rapid decrease in rotor speed.

The stator currents obtained by FLT controller are given in Figure 8(d). It can be seen that i_{sx} current controls the magnetizing current, while i_{sy} current controls the electromagnetic torque. The variation of the rotor resistance affects i_{sy} current. So, the three-phase stator currents absorbed by the machine are also affected (Figure 8(e)). In this paper, the rotor time constant T_r is variable, unlike the model with constant parameters. Figure 8(f) shows the variation of the magnetizing inductance L_m which modifies the rotor inductance $(L_r = L_{r\sigma} + L_m)$, and therefore, it allows for modification of the time constant T_r.

These results show that the control FLT is not robust with respect to the variation of the IM machine parameters. The nonrobustness is due, first, to the orientation condition (6), which assumes that the rotor resistance is constant. In

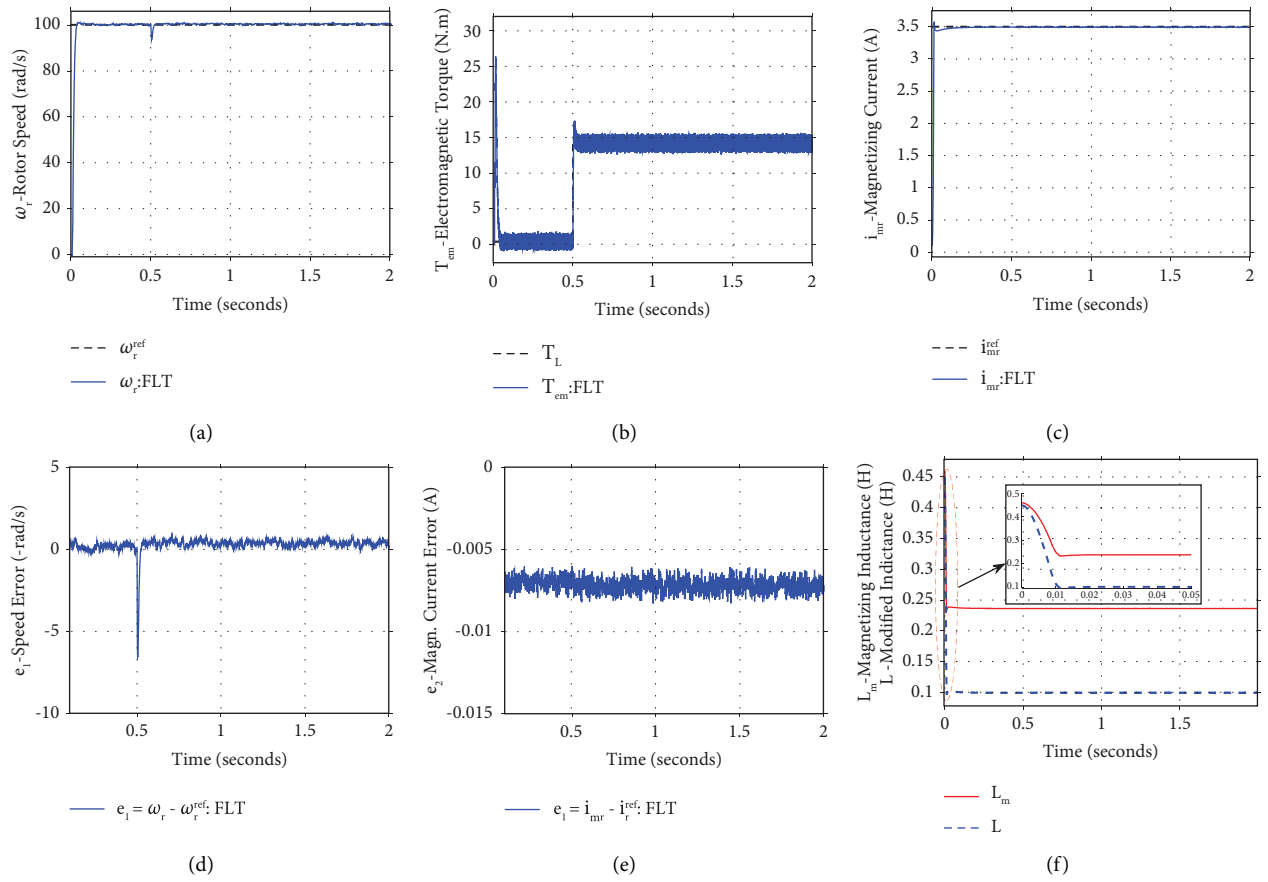

FIGURE 4: Simulation results under load torque variations (0 to 14 Nm) and constant rotor resistance ($R_r = R_{rn}$) (FLT case): (a) rotor speed, (b) electromagnetic torque, (c) magnetizing current, (d) speed error ($e_1 = \omega_r - \omega_r^{\text{ref}}$), (e) magnetizing current error ($e_2 = i_{mr} - i_{mr}^{\text{ref}}$), and (f) magnetizing inductance and modified inductance of IM.

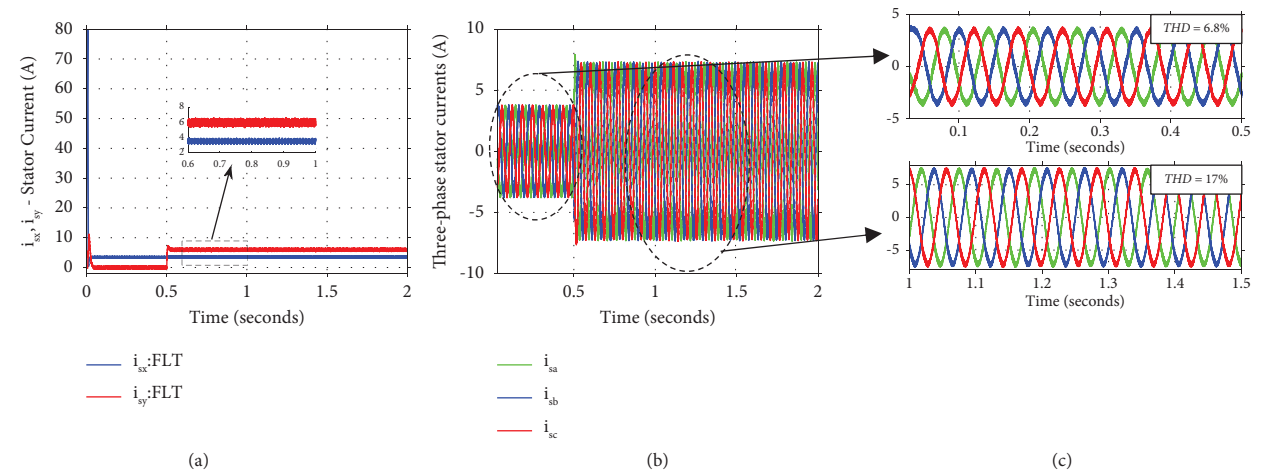

FIGURE 5: : Stator current under load torque variations (0 to 14 Nm) and constant rotor resistance ($R_r = R_{rn}$) (a) in the rotating reference frame (x, y), (b) in the (a, b, c) frame, and (c) zooming in on the three-phase currents.

reality, the rotor resistance is no longer constant; it varies according to temperature (heat). Second, because of this error in orientation, the model (7)–(10) is no longer valid, because the quadrature component of the magnetizing current will be nonzero and must be taken into account. Finally, the load torque is part of the FL control law (see equations (5) and (19)), so the accuracy of the torque estimation affects the FLT controller.

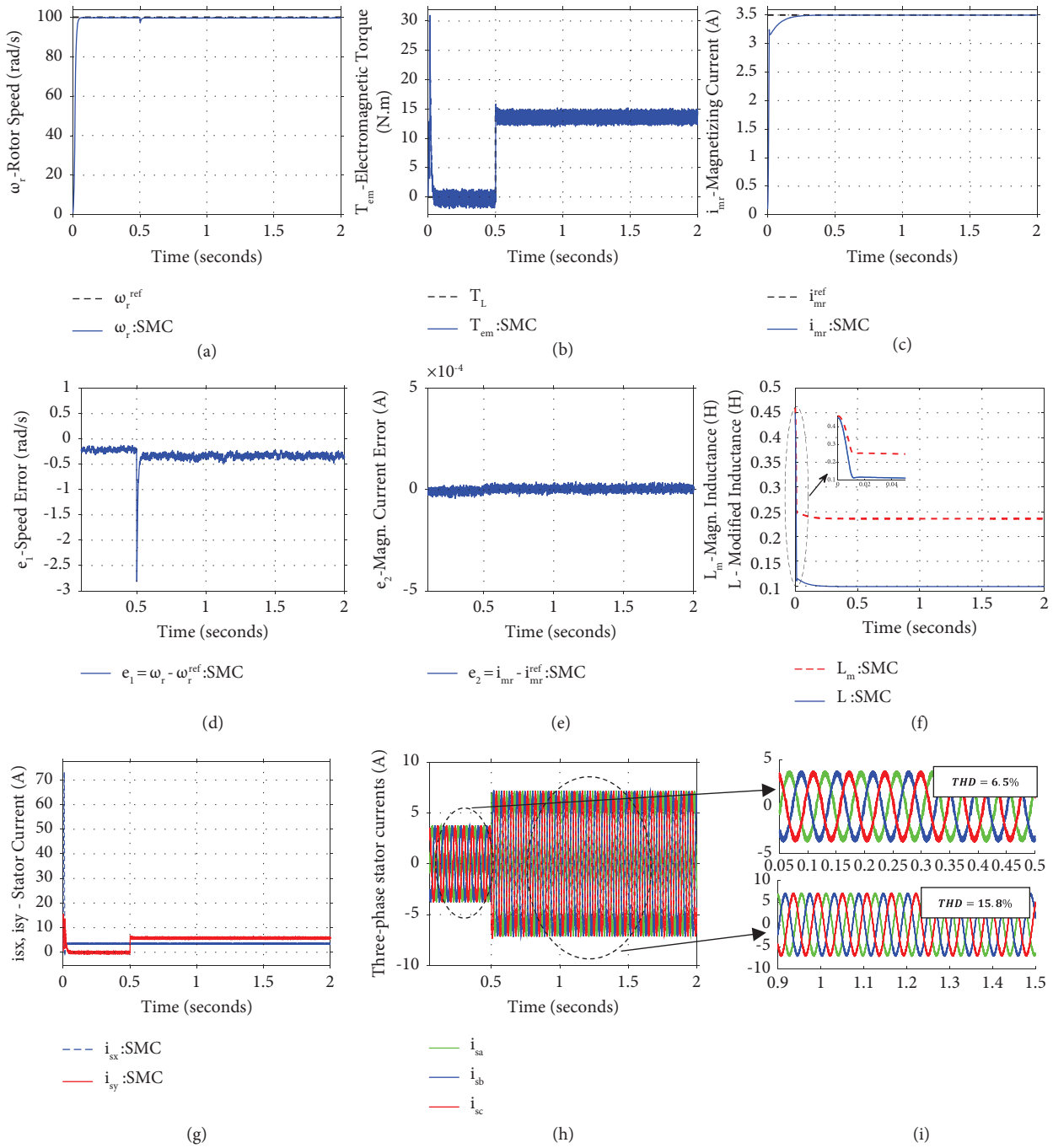

FIGURE 6: Simulation results under load torque variations (0 to 14 Nm) and constant rotor resistance ($R_r = R_{rn}$) (SMC case): (a) rotor speed, (b) electromagnetic torque, (c) magnetizing current, (d) speed error, (e) magnetizing current error, (f) magnetizing inductance and modified inductance of IM, (g) stator current in rotating frame (x, y), (h) stator current in (a, b, c) frame, and (i) zooming in on the three-phase currents.

Now, the rotor resistance varied as shown in Figure 7. Figure 9 shows the simulation results when the machine is controlled by the SMC technique.

As shown in Figure 9(a), the rotor speed accurately follows its reference even when the rotor resistance varies and in the presence of the load torque. In the case of SMC control, the electromagnetic torque is insensitive to these variations (Figure 9(b)).

The magnetizing current error is very low (on the order of 5.10^{-3}), indicating the superiority of the SMC control compared to FLT (Figure 9(c)).

It can be seen that i_{sx} current controls the magnetizing current while i_{sy} current controls the electromagnetic torque (Figure 9(d)). Unlike the FLT controller, the variation of the rotor resistance does not affect the current i_{sy}. Thus, the three-phase stator currents absorbed by the machine are not

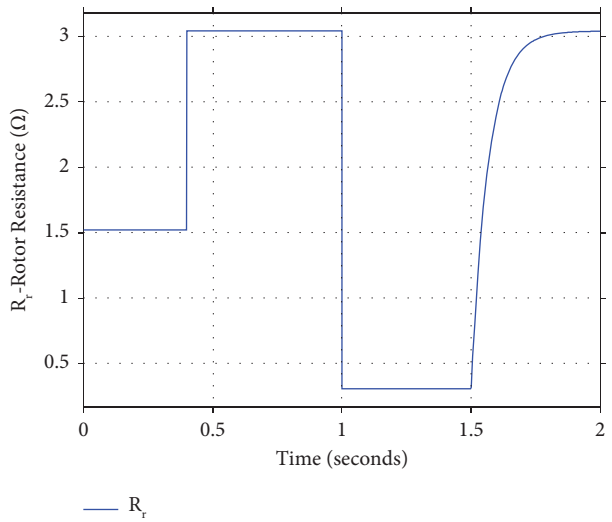

Figure 7: Profile of the rotor resistance variation.

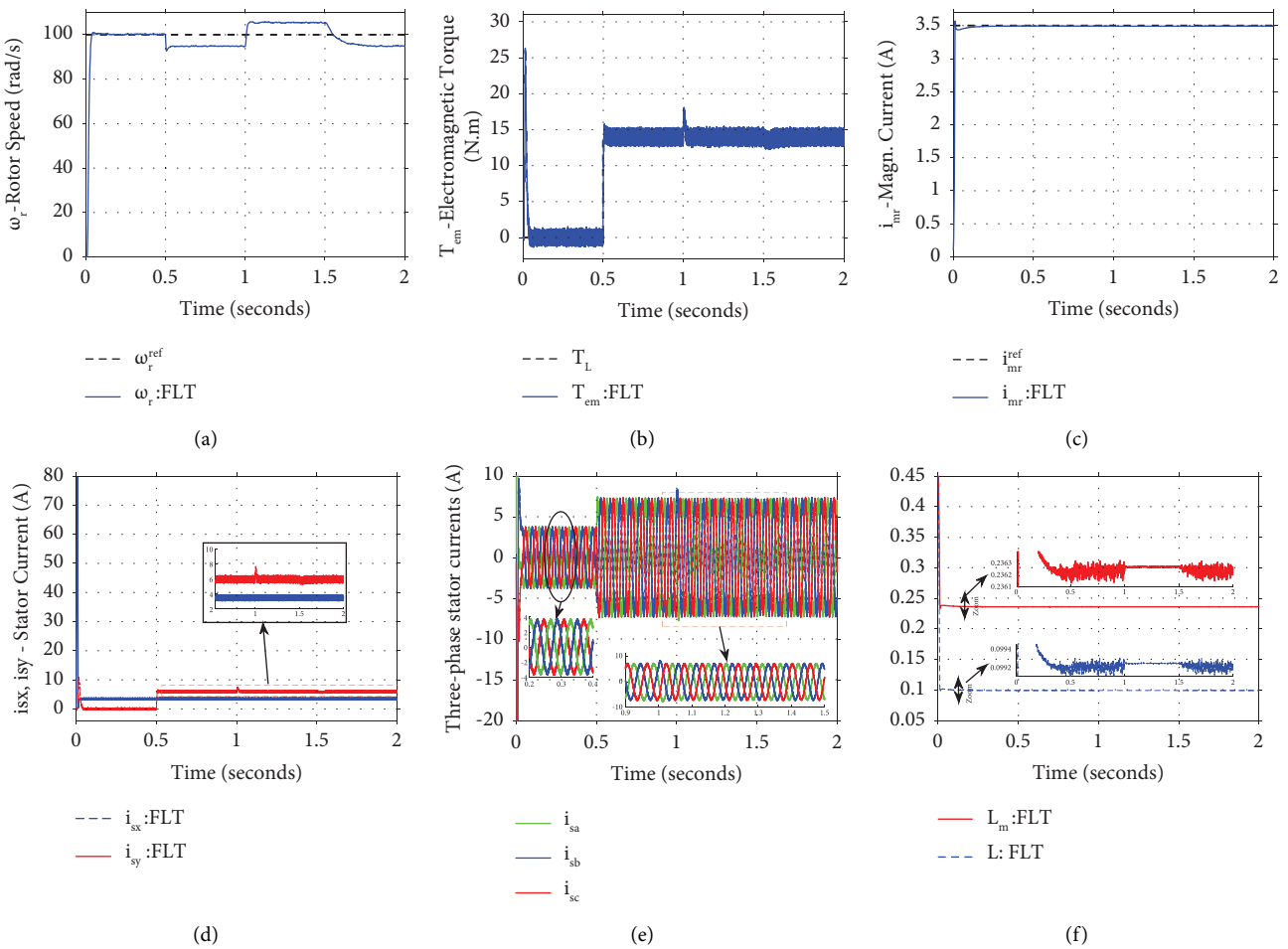

Figure 8: Simulation results under load torque (0 to 14 Nm) and rotor resistance variations (FLT controller): (a) rotor speed, (b) electromagnetic torque, (c) magnetizing current, (d) speed error ($e_1 = \omega_r - \omega_r^{\text{ref}}$), (e) magnetizing current error ($e_2 = i_{mr} - i_{mr}^{\text{ref}}$), and (f) magnetizing inductance and modified inductance of IM.

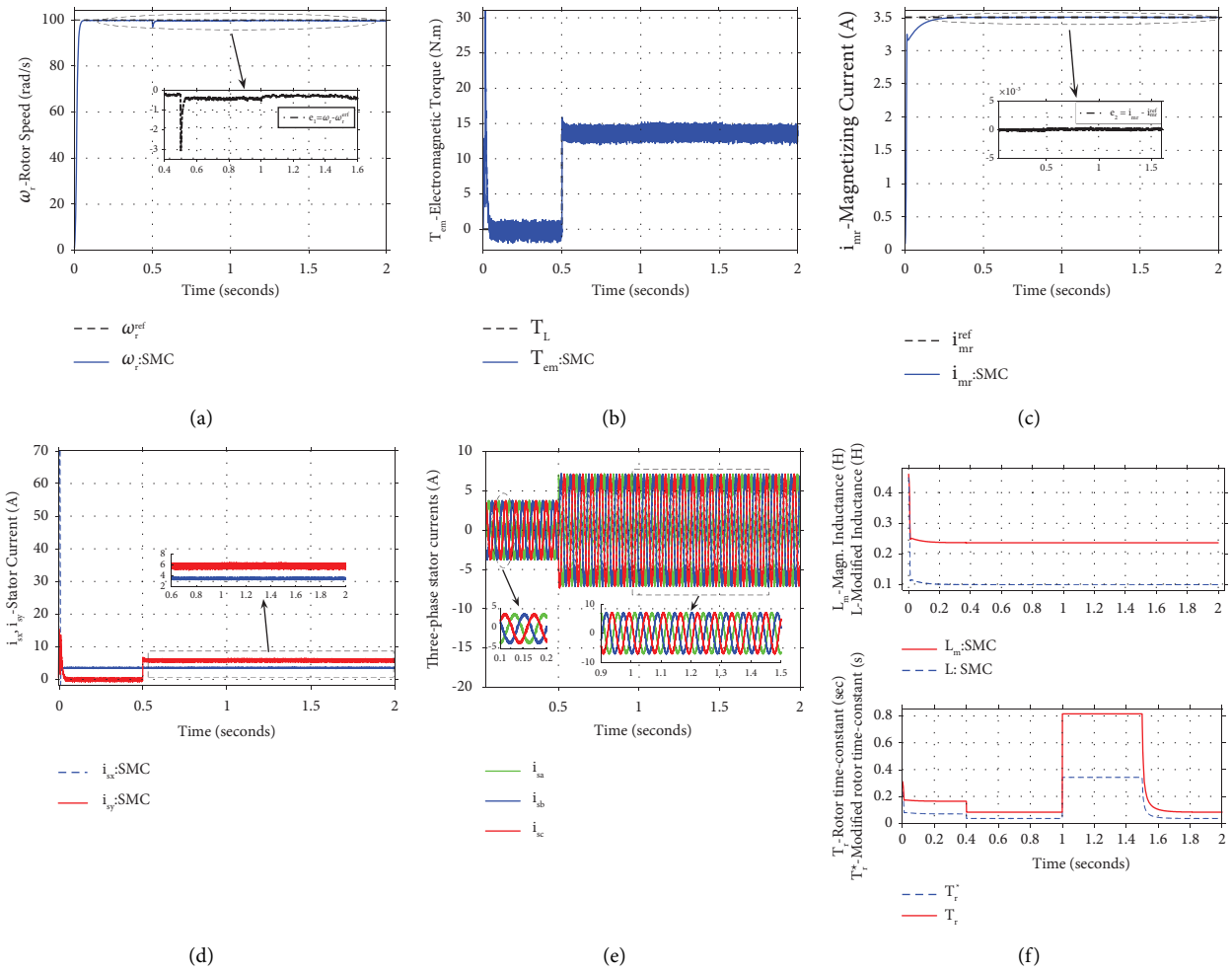

FIGURE 9: Simulation results under load torque (0 to 14 Nm) and rotor resistance variations (SMC controller): (a) rotor speed, (b) electromagnetic torque, (c) magnetizing current, (d) stator current in the rotating reference frame, (e) stator current in the (a, b, c) frame, and (f) zoom in the three-phase currents of IM.

affected either. Figure 9(f) shows the variation of the magnetizing and modified inductances (L_m, L) which modifies the rotor inductance $(L_r = L_{r\sigma} + L_m)$, and therefore it allows the modification of the time constant T_r.

Figure 10 illustrates the variation of speed, magnetizing current, and torque under an exponential variation of the rotor resistance.

When the resistance increases exponentially (Figure 10(a)), it is observed that the speed obtained by SMC accurately follows its reference with acceptable precision. However, in the FLT case, the speed tends to become negative with each speed change. As the resistance continues to increase, the precision of the speed improves in the FLT case (Figure 10(b)). The electromagnetic torque developed by the machine (Figure 10(c)) exhibits peaks during speed changes (FLT case). This phenomenon can be attributed to the fact that the speed, which tends to reverse during each speed change, adds an additional torque to the load torque. In contrast, the SMC control is unaffected by these speed changes. The stator currents show little difference, without any significant variations (Figures 10(d) and 10(e)).

As mentioned before, all inductances vary according to the magnetizing current. Figure 10(f) illustrates the variation of the magnetizing current reference, consequently resulting in variable magnetizing inductance and the rotor time constant of the machine.

It should be noted that in the SMC control law, the rotor resistance, stator resistance, and load torque are considered as disturbances. On the other hand, the machine inductances are dependent on the magnetizing inductance, which is modeled by (16). These inductances vary only with respect to the magnetizing current.

6.2.1. Remarks. In both control laws, voltages u_{sx} and u_{sy} are calculated as a function of the IM inductances $(L_r, L_s, L_m, \ldots \text{etc})$.

We can make a comparison between FL and SMC controller at several levels:

(i) Application of linear control laws: in the case of FL is easier than that of SMC

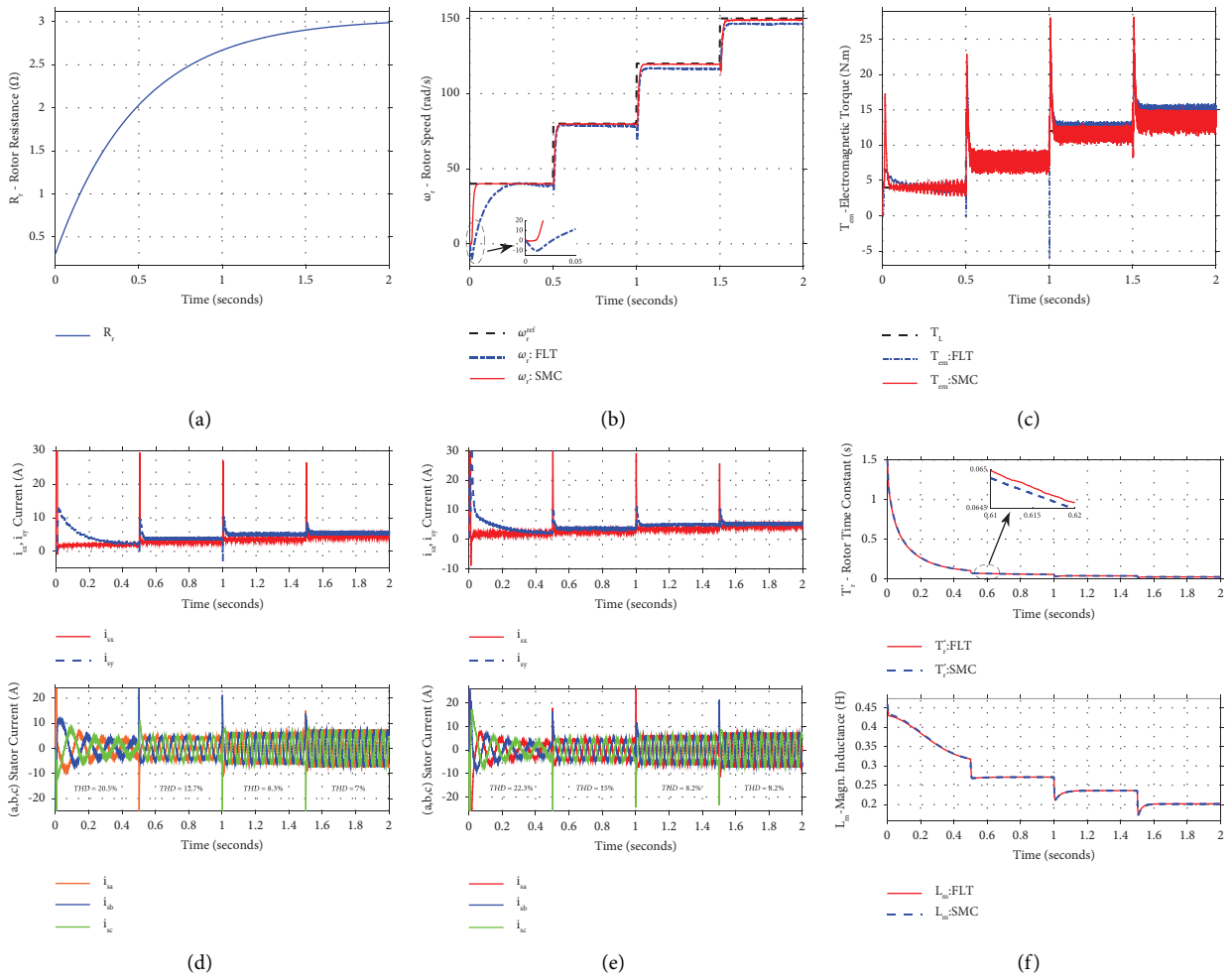

Figure 10: Simulation results under load torque and rotor resistance variations: (a): rotor resistance variation; (b) rotor speed with FLT and SMC controllers; (c) electromagnetic torque; (d) stator current (FLT case); (e) stator current (SMC case); (f) modified time constant and magnetizing inductance of IM (FLT and SMC cases).

(ii) Number of parameters to set: this number is the same in both controllers. The total is equal to four: two for the speed and two for the magnetizing current.

(iii) Robustness: the control law by SMC is more robust to the variation of IM parameters and to the estimation of some state variables. The FL controller is sensitive to these variations, and its accuracy depends on the accuracy of the flux and resistive torque observers.

(iv) The SMC controller is hindered by the requirement of significant tuning efforts, which may be perceived as a disadvantage due to their time-consuming nature. In contrast, the FL controller does not require tuning efforts, which can be considered as an advantage.

7. Conclusion

Magnetic saturation introduces variability in all parameters of the induction motor (IM), thereby increasing the nonlinearity of the machine model. The variation of rotor resistance plays a crucial role in controlling and manipulating the rotor speed. The proposed control schemes, FLT and SMC, prove to be efficient in controlling an IM while accounting for the effects of magnetic saturation and motor heating. The feedback linearization technique (FLT) provides a linear model that allows the application of linear systems theory. However, this control approach requires a higher level of accuracy in the IM model and assumes that the parameters remain constant or are precisely observable. On the other hand, sliding-mode control (SMC) is a robust technique that can effectively handle parametric variations in the IM. It offers the advantage of being simple to implement and only requiring a basic flux observer. However, the estimation of the maximum values of the disturbances occurring on the IM remains a challenge and increases the complexity of this control law.

Data Availability

No underlying data were collected or produced in this study.

Conflicts of Interest

The authors declare that they have no conflicts of interest.

References

[1] A. Kumar and T. Ramesh, "Direct field oriented control of induction motor drive," in *Proceedings of the 2015 Second International Conference on Advances in Computing and Communication Engineering*, pp. 219–223, IEEE, Dehradun, India, May 2015.

[2] A. Ba-Razzouk, A. Cheriti, and P. Sicard, "Implementation of a DSP based real-time estimator of induction motors rotor time constant," *IEEE Transactions on Power Electronics*, vol. 17, no. 4, pp. 534–542, 2002.

[3] A. Ba-Razzouk, P. Sicard, and V. Rajagopalan, "A simple on-line method for rotor resistance updating in indirect rotor flux orientation," in *Proceedings of the IEEE 2002 28th Annual Conference of the Industrial Electronics Society. IECON 02*, pp. 317–322, IEEE, Sevilla, Spain, December 2002.

[4] N. R. Klaes, "Parameter identification of an induction machine with regard to dependencies on saturation," *IEEE Transactions on Industry Applications*, vol. 29, no. 6, pp. 1135–1140, 1993.

[5] C. Attaianese, A. Damiano, G. Gatto, I. Marongiu, and A. Perfetto, "Induction motor drive parameters identification," *IEEE Transactions on Power Electronics*, vol. 13, no. 6, p. 11, 1998.

[6] D. Telford, M. W. Dunnigan, and B. W. Williams, "Online identification of induction machine electrical parameters for vector control loop tuning," *IEEE Transactions on Industrial Electronics*, vol. 50, no. 2, pp. 253–261, Apr., 2003.

[7] O. Buchholz, J. Bocker, and J. Bonifacio, "Online-identification of the induction machine parameters using the extended kalman filter," in *Proceedings of the 2018 XIII International Conference on Electrical Machines (ICEM)*, pp. 1623–1629, IEEE, Alexandroupoli, Greece, September 2018.

[8] H. Grotstollen and J. Wiesing, "Torque capability and control of a saturated induction motor over a wide range of flux weakening," *IEEE Transactions on Industrial Electronics*, vol. 42, no. 4, pp. 374–381, 1995.

[9] A. Yahiaoui and F. Bouillault, "Saturation effect on the electromagnetic behaviour of an induction machine," *IEEE Transactions on Magnetics*, vol. 31, no. 3, pp. 2036–2039, 1995.

[10] P. Vas, "Sensorless vector and direct torque control," in *Monographs in Electrical and Electronic Engineering*, Oxford University Press, Oxford, NY, USA, 1998.

[11] C. Gerada, K. J. Bradley, M. Sumner, and P. Sewell, "Evaluation and modeling of cross saturation due to leakage flux in vector-controlled induction machines," *IEEE Transactions on Industry Applications*, vol. 43, no. 3, pp. 694–702, 2007.

[12] T. Ramesh, A. Kumar Panda, and S. Shiva Kumar, "Type-2 fuzzy logic control based MRAS speed estimator for speed sensorless direct torque and flux control of an induction motor drive," *ISA Transactions*, vol. 57, pp. 262–275, 2015.

[13] M. Habbab, A. Hazzab, and P. Sicard, "Real time implementation of fuzzy adaptive PI-sliding mode controller for induction machine control," *International Journal of Energy for a Clean Environment*, vol. 8, no. 5, p. 2883, 2018.

[14] I. K. Bousserhane, A. Hazzab, M. Rahli, M. Kamli, and B. Mazari, "Direct Field-Oriented Control Design Using Backstepping Technique for Induction Motor Speed Control," in *Proceedings of the 2006 14th Mediterranean Conference on Control and Automation*, pp. 1–6, Damascus, Syria, April 2006.

[15] S. Nam and M. Uddin, "Development of an adaptive backstepping based nonlinear control of an induction motor incorporating iron loss with parameter uncertainties," in *Proceedings of the 2006 Canadian Conference on Electrical and Computer Engineering*, pp. 1662–1666, IEEE, Ottawa, ON, USA, December 2006.

[16] M. Madark, A. Ba-Razzouk, E. Abdelmounim, and M. E. Malah, "A new induction motor adaptive robust vector control based on backstepping," *International Journal of Energy for a Clean Environment*, vol. 7, no. 4, p. 1983, 2017.

[17] M.-A. Salahmanesh, H. A. Zarchi, and H. M. Hesar, "A nonlinear technique for MTPA-based induction motor drive considering iron loss and saturation effects," in *Proceedings of the 2020 11th Power Electronics, Drive Systems, and Technologies Conference (PEDSTC)*, pp. 1–6, IEEE, Tehran, Iran, February 2020.

[18] A. Ba-Razzouk, A. Cheriti, G. Olivier, and P. Sicard, "Field-oriented control of induction motors using neural-network decouplers," *IEEE Transactions on Power Electronics*, vol. 12, no. 4, pp. 752–763, 1997.

[19] M. H. Jokar, B. Abdi, and M. Ardebili, "Vector control of induction motors using radial basis function neural network," in *Proceedings of the 2007 IEEE International Symposium on Diagnostics for Electric Machines, Power Electronics and Drives*, pp. 215–218, IEEE, Cracow, Poland, September 2007.

[20] Z. Shao, Y. Zhan, and Y. Guo, "Fuzzy neural network-based model reference adaptive inverse control for induction machines," in *Proceedings of the 2009 International Conference on Applied Superconductivity and Electromagnetic Devices*, pp. 56–59, IEEE, Chengdu, China, September 2009.

[21] S. J. Plathottam and H. Salehfar, "Induction machine transient energy loss minimization using neural networks," in *Proceedings of the 2016 North American Power Symposium (NAPS)*, pp. 1–5, IEEE, Denver, CO, USA, September 2016.

[22] M. Hajian, J. Soltani, G. A. Markadeh, and S. Hosseinnia, "Adaptive nonlinear direct torque control of sensorless IM drives with efficiency optimization," *IEEE Transactions on Industrial Electronics*, vol. 57, no. 3, pp. 975–985, Mar., 2010.

[23] M. Hajian, J. Soltani, S. H. nia, and G. R. Arab, "The decoupled stator flux and torque sliding-mode control of induction motor drive taking the iron losses into account," in *Proceedings of the 2007 7th International Conference on Power Electronics and Drive Systems*, pp. 1274–1279, IEEE, Bangkok, Thailand, September 2007.

[24] J. Liu, X. You, and T. Q. Zheng, "Sliding-mode variable structure current controller for field oriented controlled linear induction motor drive," in *Proceedings of the 2009 IEEE 6th International Power Electronics and Motion Control Conference*, pp. 1036–1039, IEEE, Wuhan, China, May 2009.

[25] I. Sami, "Sliding mode-based model predictive torque control of induction machine," in *Proceedings of the 2019 International Conference on Engineering and Emerging Technologies (ICEET)*, pp. 1–5, IEEE, Lahore, Pakistan, February 2019.

[26] T. Roubache, S. Chaouch, and M. said Nait Said, "Sensorless second-order sliding mode control of Induction Motor," in *Proceedings of the 2016 5th International Conference On Systems And Control (ICSC)*, pp. 26–30, IEEE, Marrakesh, Morocco, May 2016.

[27] A. Accetta, F. Alonge, M. Cirrincione, M. Pucci, and A. Sferlazza, "Feedback linearizing control of induction motor

considering magnetic saturation effects," *IEEE Transactions on Industry Applications*, vol. 52, no. 6, pp. 4843–4854, 2016.

[28] F. Alonge, M. Cirrincione, M. Pucci, and A. Sferlazza, "Input-output feedback linearization control of linear induction motors including the dynamic end-effects," in *Proceedings of the 2014 IEEE Energy Conversion Congress and Exposition (ECCE)*, pp. 3562–3569, IEEE, Pittsburgh, PA, USA, September 2014.

[29] F. Alonge, M. Cirrincione, M. Pucci, and A. Sferlazza, "A nonlinear observer for rotor flux estimation of induction motor considering the estimated magnetization characteristic," *IEEE Transactions on Industry Applications*, vol. 53, no. 6, pp. 5952–5965, 2017.

[30] Marino, *Induction Motor Control Design*, Springer, London, UK, 2010.

[31] T. Tuovinen, M. Hinkkanen, and J. Luomi, "Modeling of saturation due to main and leakage flux interaction in induction machines," *IEEE Transactions on Industry Applications*, vol. 46, no. 3, pp. 937–945, 2010.

[32] M. Pucci, "State-space space-vector model of the induction motor including magnetic saturation and iron losses," *IEEE Transactions on Industry Applications*, vol. 55, no. 4, pp. 3453–3468, 2019.

[33] A. Accetta, F. Alonge, M. Cirrincione, M. Pucci, and A. Sferlazza, "Parameter identification of induction motor model by means of state space-vector model output error minimization," in *Proceedings of the 2014 International Conference on Electrical Machines (ICEM)*, pp. 843–849, IEEE, Berlin, Germany, September 2014.

[34] M. Madark, A. Ba-razzouk, E. Abdelmounim, and M. El Malah, "Adaptive backstepping control of induction motor powered by photovoltaic generator," *International Journal of Energy for a Clean Environment*, vol. 11, no. 4, p. 2842, 2021.

[35] D.-W. Chung, Joohn-Sheok Kim, and S. K. Sul, "Unified voltage modulation technique for real-time three-phase power conversion," *IEEE Transactions on Industry Applications*, vol. 34, no. 2, pp. 374–380, 1998.